Amintas *et al. Journal of Biological Engineering* (2024) 18:53
https://doi.org/10.1186/s13036-024-00450-3

Journal of Biological Engineering

METHODOLOGY

Open Access

Integrating allele-specific PCR with CRISPR-Cas13a for sensitive *KRAS* mutation detection in pancreatic cancer

Samuel Amintas[1,2*†], Grégoire Cullot[3,4†], Mehdi Boubaddi[1,5], Julie Rébillard[1], Laura Karembe[1], Béatrice Turcq[3,6], Valérie Prouzet-Mauléon[3,6], Aurélie Bedel[1,7], François Moreau-Gaudry[1,7], David Cappellen[1,2] and Sandrine Dabernat[1,7*]

Abstract

Background The clustered regulatory interspaced short palindromic repeats (CRISPR)-Cas13a system has strong potential for highly sensitive detection of exogenous sequences. The detection of $KRAS^{G12}$ point mutations with low allele frequencies may prove powerful for the formal diagnosis of pancreatic ductal adenocarcinoma (PDAC).

Results We implemented preamplification of *KRAS* alleles (wild-type and mutant) to reveal the presence of mutant *KRAS* with CRISPR-Cas13a. The discrimination of $KRAS^{G12D}$ from $KRAS^{WT}$ was poor for the generic *KRAS* preamplification templates and depended on the crRNA design, the secondary structure of the target templates, and the nature of the mismatches between the guide and the templates. To improve the specificity, we used an allele-specific PCR preamplification method called CASPER (Cas13a Allele-Specific PCR Enzyme Recognition). CASPER enabled specific and sensitive detection of $KRAS^{G12D}$ with low DNA input. CASPER detected *KRAS* mutations in DNA extracted from patients' pancreatic ultrasound-guided fine-needle aspiration fluid.

Conclusion CASPER is easy to implement and is a versatile and reliable method that is virtually adaptable to any point mutation.

Keywords CRISPR, Cas13a, *KRAS*, Pancreatic cancer, Liquid biopsy

Background

The clustered regulatory interspaced short palindromic repeats (CRISPR)-Cas13a system was shown very potent and sensitive for the detection of exogenous sequences in human samples. For example, CRISPR-Cas13a coupled with fluorescent reporters was designed to detect specific RNA target sequences and was first applied to virus and bacterial genome detection with extremely high sensitivity (aM, [1]). To establish its potential for use in oncology, we previously used CRISPR-Cas13a to detect large, cancer-specific genomic alterations, such as $EGFR^{VIII}$ fusion variants or *EGFR* exon 19 deletions, for which performance is required under clinical conditions [2]. These large rearranged sequences can be considered exogenous

†Samuel Amintas and Grégoire Cullot contributed equally to this work.

*Correspondence:
Samuel Amintas
samuel.amintas@u-bordeaux.fr
Sandrine Dabernat
sandrine.dabernat@u-bordeaux.fr
[1] Bordeaux Institute in Oncology – BRIC – BioGo team, Univ. Bordeaux, INSERM U1312, Bordeaux, France
[2] Department of Tumor Biology and Tumor Library, CHU Bordeaux, Bordeaux, France
[3] Bordeaux Institute in Oncology – BRIC – MoTRIL team, Univ. Bordeaux, INSERM U1312, Bordeaux, France
[4] Department of Biology, ETH Zurich, Zurich, Switzerland
[5] Department of Digestive Surgery, CHU Bordeaux, Bordeaux, France
[6] CRISP'edit, TBMCore, CNRS UAR3427, INSERM US005, Bordeaux, France
[7] Department of Biochemistry and Molecular Biology, CHU Bordeaux, Bordeaux, France

since they are unique in the pathological genome and are absent in healthy genomes. CRISPR-Cas13a was also successful in distinguishing single nucleotide polymorphisms (with an allele frequency of 50%, [1]). Point mutations occurring during oncogenesis can display very low allele frequencies, depending on the sample type, clonal frequency, or tumor heterogeneity. The sensitivity of CRISPR-Cas13a seems promising for detecting such rare sequences in any challenging molecular situation, such as liquid biopsy or molecular residual disease follow-up in cancer patients.

Pancreatic ductal adenocarcinoma (PDAC) suffers from a late diagnosis due to asymptomatic tumor growth and nonspecific symptoms. Before any treatment is administered, the carcinoma nature of the lesions is often confirmed by cytopathological analysis. Endoscopic ultrasound-guided fine-needle aspiration (EUS-FNA), which provides tissue biopsies, is risky [3] and has a low negative predictive value for delaying diagnosis [4]. The inconclusive or doubtful results obtained by the EUS-FNA cytopathological exam are strongly related to the scarcity of tumor cells in the samples.

The molecular diagnosis of PDAC was developed by improving the sensitivities of nucleic acid-based methods. Oncogenic *KRAS* mutation represents one of the most frequent genetic events in tumors, particularly in the adenocarcinoma subtype.[5]. In this respect, PDAC is of particular interest since > 90% of tumors present *KRAS* mutations [6]. The exploration of *KRAS* mutation status by PCR in the primary tumor coupled with cytology slightly improved the diagnostic performance [7–9], confirming the hypothesis that *KRAS* mutation detection participates in confirming the cancerous nature of the lesion and expedites therapeutic decisions. Nevertheless, intense desmoplastic reactions dilute informative tumor cells in fibrosis, highlighting the need for highly sensitive detection methods. Ideally, strategies should be simple and cost-effective to make the detection of any mutation easily implementable.

This study challenged the detection of 3 frequent *KRAS* mutations (G12D, G12V, and G12C, respectively accounting for 50%, 30%, and 2% of $KRAS^{mut}$ PDAC tumors [10]) by CRISPR-Cas13a using different crRNA guide designs and after KRAS preamplification. To improve allele discrimination, we adapted a system combining Cas13a detection sensitivity with allele-specific PCR amplification to propose CASPER (Cas13a Allele-Specific PCR Enzyme Recognition), a new versatile, easy-to-implement, and highly sensitive method for detecting low-frequency point mutations.

Methods

Reagents and enzymes

The LwaCas13a enzyme was obtained from GenScript and stored at -80 °C in 50 mM Tris–HCl, 600 mM NaCl, 5% glycerol, and 2 mM DTT, pH 7.5. PAGE Ultramer DNA oligos for RNA guide synthesis were obtained from Integrated DNA Technologies (IDT, United States). A HiScribe™ T7 Quick High Yield RNA Synthesis Kit containing T7 polymerase, RNase inhibitor, and NTP mix buffer was obtained from New England Biolabs (NEB, United States). PCR primers were obtained from Eurogentec (Belgium). Hydroxyethyl piperazine ethane sulfonic acid (HEPES) and dimethylsulfoxide (DMSO) were obtained from Sigma–Aldrich (United States).

Cell culture

BxPC-3, AsPC-1, and MIA PaCa-2 cells were maintained in Dulbecco's minimal essential medium (DMEM, Invitrogen, Saint Aubin, France), and Capan-1 cells were maintained in Roswell Park Memorial Institute (RPMI, Invitrogen). For both media, 10% fetal bovine serum (FBS, Invitrogen), 100 U/mL penicillin (Invitrogen), and 100 µg/mL streptomycin (Invitrogen) were added. All cell lines were cultured at 37 °C and 5% CO_2 in a humidified chamber.

Patient inclusion and sample collection

Patients were recruited prospectively between February 2023 and March 2023. All patients who received endoscopic ultrasound-guided fine needle aspiration (EUS-FNA) in the context of a pancreatic mass during these 2 months were recruited. The patients' demographic information is summarized in Table 1.

DNA extraction and quantification

DNA samples for *KRAS* detection were extracted from pancreatic tumor cell lines using a QIAamp DNA Extraction Kit® (Qiagen, France). $KRAS^{WT/WT}$ DNA and $KRAS^{G12D/G12D}$, $KRAS^{G12C/G12C}$, and $KRAS^{G12V/G12V}$ mutant DNA were extracted from the BxPC-3, AsPC-1, MIA PaCa-2, and Capan-1 cell lines, respectively, and verified by NGS analysis using the Bordeaux University Hospital Tumor Biology Department routine solid tumor panel (custom AmpliSeq panel with an Ion Torrent S5 sequencer (Thermo Fisher Scientific, United States)). All DNA samples were quantified by spectrophotometry using a Nanodrop® One/One device (Thermo Fisher Scientific, United States). For molecular analysis of the needle-rinsing fluids, a Maxwell RSC ccfDNA Plasma Kit was used for DNA extraction, and a DS11FX automated system (DeNovix) was used for concentration evaluation. The patient sample DNA concentrations are reported in Supplemental Table 1.

Table 1 Patient demographics

Patients	*n* = 24
Age	72.5 (51–89)
Sex	
Male	16 (66.7%)
Female	8 (33.3%)
IMC (kg/m2)	25 (15–36)
ASA	
1	3 (12.5%)
2	14 (58.3%)
3	7 (29.2%)
Symptoms	
Pain	11 (45.8%)
Jaundice	11 (45.8%)
Altered General Condition	21 (87.5%)
Unbalanced diabetes	3 (12.5%)
Incidental	2 (8%)
Tumor localization	
Head	16 (66.8%)
Body	5 (20.8%)
Tail	2 (8.4%)
Suspected Diagnosis	
Ductal Adenocarcinoma	21 (87.5%)
Degenerated IPMNs	1 (4.1%)
Auto Immune	1 (4.1%)
Ampulloma	1 (4.1%)

ASA American Society of Anesthesiologists classification, *IPMNs* Intraductal Papillary Mucinous Neoplasms

RNA guide synthesis and purification

Guide RNAs were produced by T7-mediated in vitro transcription as described by *Kellner* et al. [11]. Briefly, oligonucleotides (PAGE Ultramer DNA oligos from Integrated DNA Technologies) were resuspended at a concentration of 100 µM. Annealing was performed at 95 °C for 5 min, followed by a slow temperature decrease to 4 °C (0.1 °C/s) using common forward p.T7 oligo and Taq buffer (10X). In vitro transcription was next performed overnight with the HiScribe™ T7 Quick High Yield RNA Synthesis Kit (NEB, MA, USA) following the manufacturer's instructions, and the products were subsequently purified with Agencourt RNAClean XP beads (Beckman Coulter). Purified RNA products were aliquoted and frozen at -80 °C.

DNA amplification step

PCR and allele-specific PCR amplification were performed using Phire Tissue Direct PCR Master Mix® (Thermo Fisher Scientific) following the manufacturer's instructions. The amplification primers and related annealing temperatures used are listed in Supplemental Table 2. All amplifications were performed using 10 ng of gDNA input, except for patient samples with insufficient DNA concentrations (Supplemental Table 1). An overhang including the T7 promoter was used to enable subsequent T7-mediated in vitro transcription of the PCR products [11]. All primers were used at a concentration of 250 nM. By default, 35 cycles of amplification were performed. For CASPER, after multiple conditions were tested, only 30 cycles of amplification were performed to optimize specificity.

CRISPR-Cas13a detection step

The RNA guide spacer sequences used are listed in Supplemental Table 2 and Supplemental Figs. 1 to 5. In vitro transcription of *KRAS* PCR products and Cas13-mediated detection of T7-produced RNA were performed simultaneously as described previously [11]. The detection mixture included 16 mM HEPES, 7.2 mM $MgCl_2$, 640 nM rNTP, 0.05 U/µL T7 RNA polymerase, 1.6×10^3 U/µL murine RNase inhibitor (NEB), 5 µg/µL LwaCas13a protein, 400 pg/µL RNA guide, and 100 nM fluorescent RNA reporter. The final volume of the reaction was 20 µl, which included 1 µL of PCR products. All manipulations were performed on ice. After the addition of PCR products, the samples were immediately transferred to a CFX96 Touch Real-Time PCR Detection System (Bio-Rad), and the fluorescence level was quantified every minute for 90 min. Analysis of the results was performed using CFX MaestroTM software (Bio-Rad). The fluorescence intensity ratio was calculated at 90 min as follows:

$$\frac{(Mutanttemplatefluorescenceat90min - Mutanttemplatefluorescenceat1min)}{(WTtemplatefluorescenceat90min - WTtemplatefluorescenceat1min)}$$

Real-time quantitative PCR

The detection of the $KRAS^{G12D}$ and $KRAS^{WT}$ alleles was performed using a Promega GoTaq® qPCR kit (Promega, Wisconsin) following the manufacturer's instructions with 10 ng of DNA input. The primers used and annealing temperatures are summarized in Supplemental Table 2. All primers were used at a concentration of 2.5 µM. By default, 35 cycles of amplification were performed. The data were analyzed with CFX Maestro Software (Bio-Rad). The relative expression of the

KRAS^{G12D} and *KRAS*^{WT} alleles was first normalized to that of GAPDH and then represented as fold changes ($2^{-\Delta\Delta Ct}$). Melting curves showed that primers amplified only the specific fragments.

Droplet digital PCR

Droplet digital PCR analyses were performed on the Bio-Rad ddPCR platform (Bio-Rad, United States) with a QX-200 TM droplet generator and a QX-200 TM droplet reader. Bio-Rad KRAS G12/G13 screening and Bio-Rad KRAS G12D-specific kits were used for global or specific *KRAS*^{G12} mutant detection according to the manufacturer's instructions. To compare the performance of ddPCR vs. PCR-CRISPR-Cas13a or CASPER, all experiments were performed using 10 ng of DNA. For patient samples, various amounts of DNA (18 µL, regardless of DNA concentration) were used for the KRAS G12/13 multiplex ddPCR screening assay, and 10 ng was used for the KRAS G12D-specific ddPCR assay, except for patient samples with insufficient DNA concentrations (Supplemental Table 1). Analysis of the results was performed using QuantaSoftTM software (Bio-Rad) with laboratory-validated clinical routine interpretation guidelines. For each assay, a *wild-type* sample and a "no DNA input" control were analyzed. The MAF positivity threshold (0.056%) was previously determined [12]. A sample was considered positive when the lower standard deviation value of the MAF was greater than the positivity threshold.

RNA secondary structure analysis

The predicted secondary RNA structures of the *KRAS* T7 RNA products were obtained with RNAfold® software (http://rna.tbi.univie.ac.at/cgi-bin/RNAWebSuite/RNAfold.cgi). The default parameters were used.

Statistical analysis

Statistical tests were performed using Graph-Pad Prism software (v6.04). The results are expressed as the mean ± SEM or mean ± SD and were analyzed by unpaired, bilateral Student's t tests with Welch's correction. Correlation analyses were performed using Spearman's test. $p < 0.05$ was considered to indicate statistical significance.

Results

KRAS allele discrimination by CRISPR-Cas13a using crRNA guides hybridization of the mutant nucleotide at position 19 of the spacer sequence

We first used the CRISPR-Cas13a platform to detect the most frequent alleles, *KRAS*^{G12D}, *KRAS*^{G12V}, and *KRAS*^{G12C}, using a crRNA design previously reported to efficiently target *KRAS*^{G12D} mRNAs *in cellulo* [13] (Fig. 1a). As authors obtained the maximum specificity for the KRAS^{G12D} allele using crRNA with mutation recognition site in position 19 of the spacer sequence, we first tested the in vitro discrimination ability of crRNA19^{G12X} guides (with the discriminative nucleotide position placed on the 19th nucleotide of the spacer crRNA sequence), which perfectly matched the mutant allele and presented one mismatch with the *WT* allele (SupplementalFig. 1a-c). Cas13a collateral RNase activity on reporter fluorescent RNA probes was induced by all 3 guides, but the guides also hybridized to the *WT* allele (Fig. 1b-d**,** blue bars and curves). Noticeably, discrimination variations were observed between the guides, with crRNA19^{G12C} bearing the best specificity, with a maximal fluorescence intensity ratio to *WT* detection of 11.5 ± 3.5 times (versus 2.1 ± 0.5 for crRNA19^{G12V} and 1.5 ± 0.1 for crRNA19^{G12D}).

Due to the low specificity observed in the initial basic crRNA design, and as previously described by *Zhao* et al. [13], we introduced a mismatch at position 14 to obtain crRNA19^{G12X}-14, which presented 1 mismatch with the mutant allele and 2 mismatches with the *WT* allele (Supplemental Fig. 2a-c). The synthetic mismatch at position 14 slightly improved the detection of *KRAS*^{G12D} (a maximal fluorescence intensity ratio of 2.2 ± 0.3 versus 1.5 ± 0.1), did not change the detection of *KRAS*^{G12C} (a maximal ratio of 9.9 ± 1.8), but diminished the detection of *KRAS*^{G12V} (1.4 ± 0.1 versus 2.1 ± 0.5) (Fig. 2a-c).

As the addition of one synthetic mismatch placed around the discriminative nucleotide position differentially impacted the *WT*/mutation discrimination [11], we produced a guide with 2 synthetic mismatches with the mutant *KRAS*^{G12D} allele and 3 mismatches with the *WT* allele (Supplemental Fig. 2d). The specificity of crRNA19^{G12D}-14–18 was unchanged (fluorescence ratio of 2.3 ± 0.1, Supplemental Fig. 2e). Thus, although position 19 may distinguish *KRAS*^{G12C} from KRAS^{WT} with some specificity, the discrimination of the *WT* and *KRAS*^{G12D} alleles is not sufficient, even when 3 mismatches are present between the crRNA guide and the *WT* template.

KRAS allele discrimination by CRISPR-Cas13a using crRNA guides hybridization of the mutant nucleotide at position 12 of the spacer sequence

The "seed" region of the crRNA spacer sequence, covering nucleotides 5 to 15, is described as more sensitive to mismatches [1]. We thus designed crRNA12^{G12D} (Supplemental Fig. 3a). The specificity was slightly greater than that of crRNA19^{G12D} (the maximal fluorescence intensity ratio to the *WT* signal was 2.0 ± 0.2 versus 1.5 ± 0.1) but was not sufficient for full discrimination (Fig. 3a). Indeed, using CRISPR-Cas13a for low-frequency mutant allele detection implies the absence of reporter RNA cleavage by Cas13a with the *WT* template. Introduction of synthetic mismatches (crRNA12^{G12D}-13 and

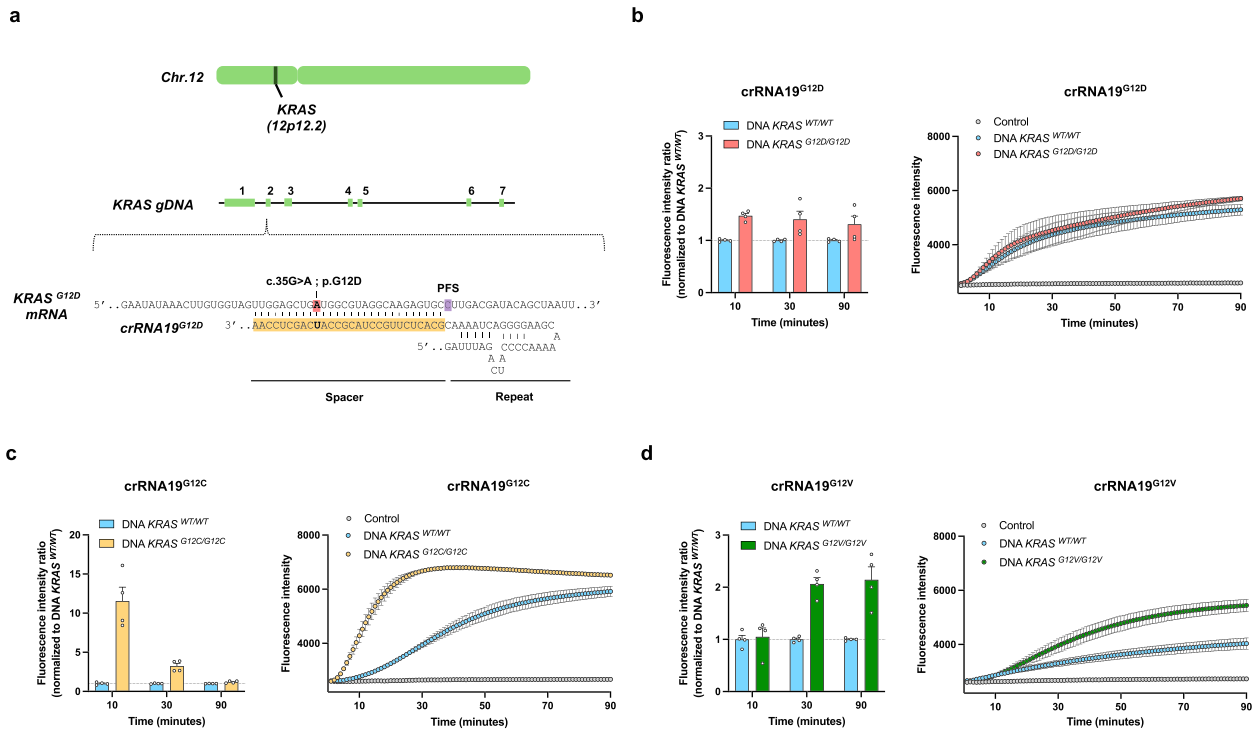

Fig. 1 crRNA19 for *KRAS*^{G12X} allele detection by CRISPR-Cas13a. **a** (Top) Chromosomal location and detailed view of the *KRAS* gene. (Bottom) The sequence of mutated *KRAS*^{G12D} RNA products (obtained after T7-mediated in vitro transcription) and the crRNA-19 G12D spacer sequence (highlighted in light yellow). The c.35G > A point mutation is shown in red. The protospacer flanking site (PFS) is highlighted in purple. **b-d** Fluorescence ratio (left) and fluorescence level over time (right) in the presence of crRNA19^{G12D} (**b**), crRNA19^{G12C} (**c**) or crRNA19^{G12V} (**d**) and PCR products from matching *KRAS* mutants or *KRAS*$^{WT/WT}$. **b-d** Results are presented as the mean ± SEM with $n = 4$ replicates from independent experiments

crRNA12^{G12D}-13–11, Supplemental Fig. 3b,c) did not fully discriminate alleles (a maximal fluorescence ratio to the *WT* signal of 1.6 ± 0.05 and 2.0 ± 0.6, respectively) and resulted in a global loss of signal for crRNA12^{G12D}-13–11 (Fig. 3b,c). We also tested whether a recognition site placed at the 5' extremity of the spacer sequence, like it was describe in the publication of *Kellner* et al. [11], could diminish the recognition of the *KRAS*^{WT} allele and designed crRNA4^{G12D} (Supplemental Fig. 3d). Like for crRNA19^{G12D}, crRNA4^{G12D} did not present any specificity for the *KRAS*^{G12D} allele (a maximal fluorescence intensity ratio of 1.1 ± 0.1, Supplemental Fig. 3e).

We next challenged the crRNA12^{G12D} guide with sensitivity experiments on serially diluted DNA samples. The sensitivity of CRISPR-Cas13a was 10%, while conventional ddPCR was tenfold more sensitive (Fig. 3d and Supplemental Fig. 3f).

KRAS allele discrimination by CRISPR-Cas13a using hairpin spacer crRNA guides

Hairpin-spacer crRNA guides feature an additional sequence downstream of the spacer, which competes for hybridization with the spacer either on the target DNA (mutant or *WT*) or with the spacer itself. This competition, aided by hairpin structures, may minimize binding to the *WT* allele while maintaining sufficient binding to the mutant allele (Fig. 4a). With the discriminative nucleotide position still placed on the 12th nucleotide, we designed 3 different hairpin-spacer crRNAs with or without additional synthetic mismatches (Supplemental Fig. 4a-c). The hairpin spacer guides were not able to fully discriminate *KRAS* alleles (Fig. 4b-d) or increase sensitivity compared with crRNA12^{G12D} (Fig. 4e).

CASPER: Coupling CRISPR-Cas13a sensitivity and allele-specific PCR specificity

Among the CE-in vitro diagnostic (CE-IVD) platforms offering highly specific identification of single nucleotide variants (SNPs) and ddPCR, allele-specific (AS)-based methods provide good performance [14]. However, the limit of detection highly depends on the DNA input [15]. Here, we tested the potential of CRISPR-Cas13a for the identification of low-frequency *KRAS* mutant alleles in a limited DNA quantity (10 ng), compatible with liquid biopsy circulating-free DNA (cfDNA) analysis or other applications with low DNA input. The routinely used

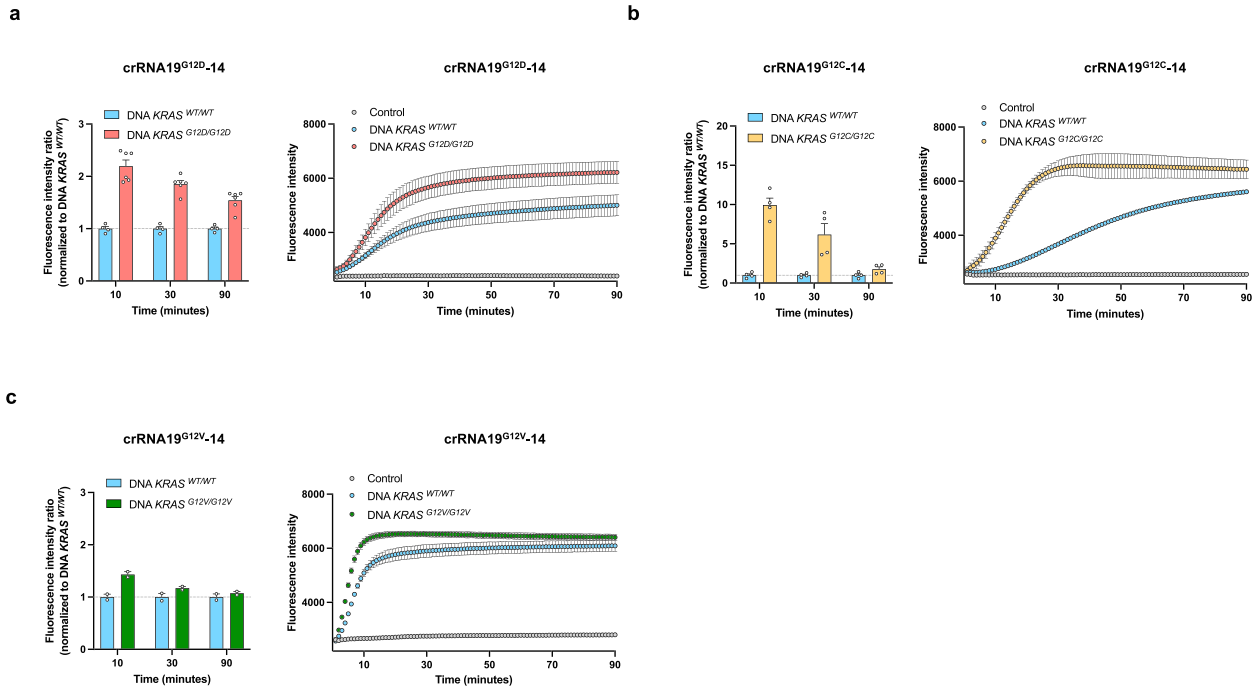

Fig. 2 crRNA19-14 for KRAS^{G12X} allele detection by CRISPR-Cas13a. **a-c** Fluorescence ratio (left) and fluorescence level over time (right) in the presence of crRNA19^{G12D}-14 G12D (**a**), crRNA19^{G12C}-14 (**b**), or crRNA19^{G12V}-14 (**c**) and PCR products from matching KRAS mutations or KRAS$^{WT/WT}$. **a-c** The results are presented as the mean ± SEM of $n = 6$ (**a**), $n = 4$ (**b**) and $n = 2$ (**c**) replicates from independent experiments

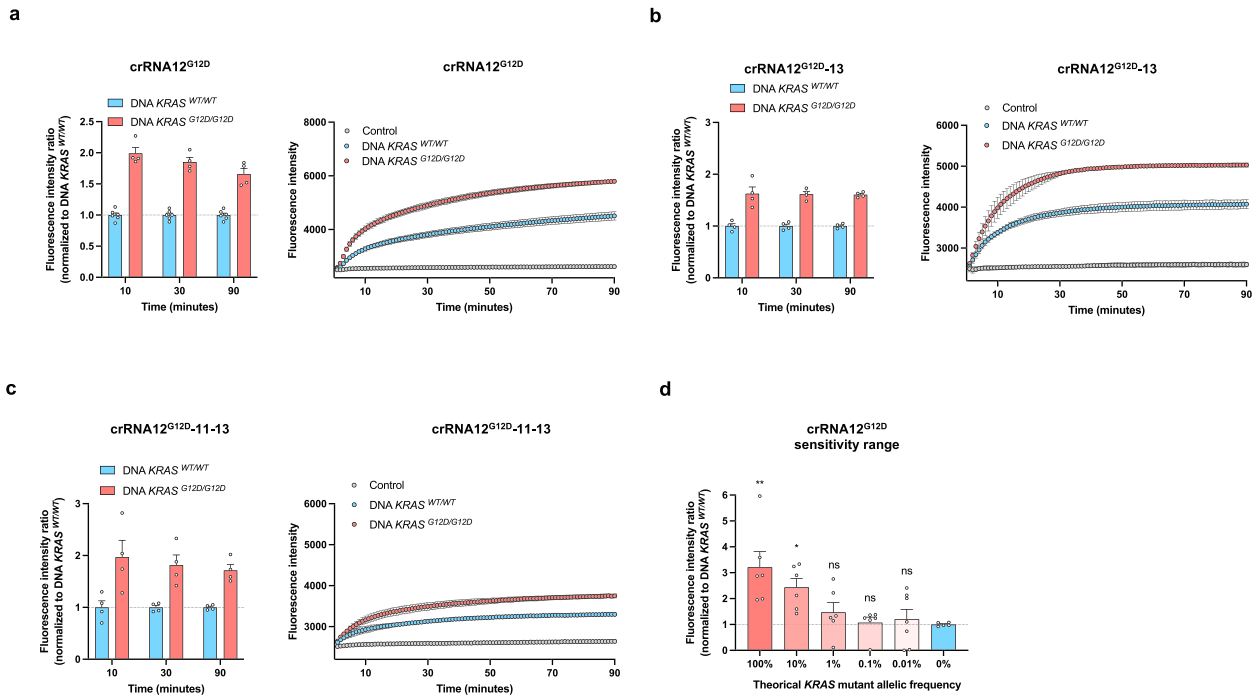

Fig. 3 crRNA12 for KRAS^{G12D} allele detection by CRISPR-Cas13a. **a-f** Fluorescence ratio (left) and fluorescence level over time (right) in the presence of crRNA12^{G12D} (**a-f**), crRNA12^{G12D}-13 (**b**), crRNA12^{G12D}-11–13 (**c**), and PCR products from KRAS$^{G12D/G12D}$ or KRAS$^{WT/WT}$. **d** Quantification of the fluorescence ratio at 90 min in the presence of crRNA12^{G12D} and PCR products from KRAS^{G12D} DNA diluted in KRAS^{WT} DNA. **a-d** Results are presented as the mean ± SEM with $n = 6$ (**a-b**), $n = 4$ (**c**) and $n = 3$ (**d**) replicates from independent experiments. *: $p < 0.05$; **: $p < 0.01$; ns: not significant

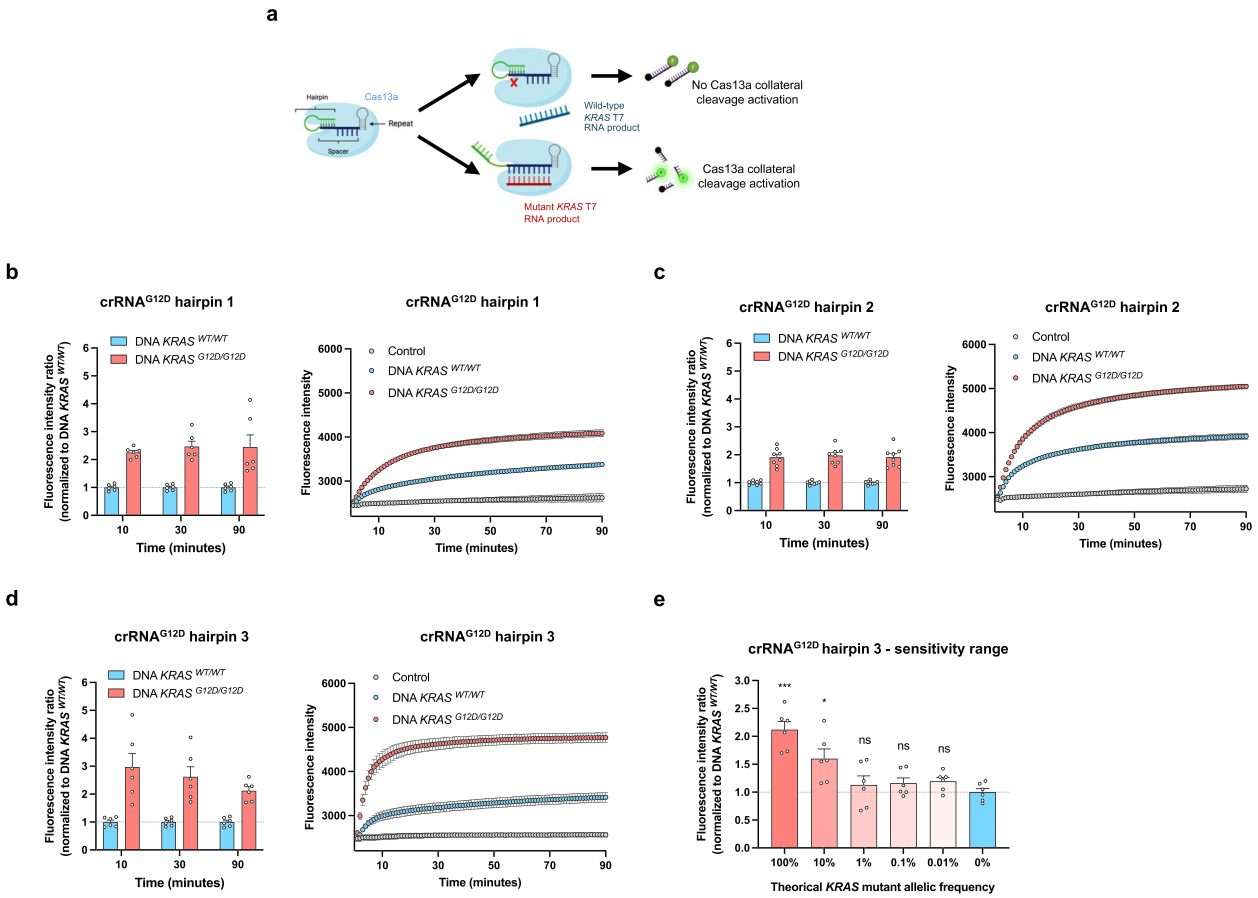

Fig. 4 Hairpin crRNA for KRAS^{G12D} allele detection by CRISPR-Cas13a. **a** Illustration of the crRNA^{G12D} hairpin system. **b-d** Fluorescence ratio (left) and fluorescence level over time (right) in the presence of crRNA^{G12D} hairpin 1 (**b**), crRNA^{G12D} hairpin 2 (**c**) or crRNA^{G12D} hairpin 3 (**d**) and PCR products from the KRAS$^{G12D/G12D}$ mutation or KRAS$^{WT/WT}$. **e** Quantification of the fluorescence ratio at 90 min in the presence of crRNA^{G12D} hairpin 3 and PCR products from KRAS^{G12D} DNA diluted in KRAS^{WT} DNA. **b-d** The results are presented as the mean ± SEM, with $n = 6$ (**b, d**) and $n = 8$ (**c**) replicates from independent experiments. **e** Results are presented as the mean ± SEM with $n = 6$ replicates from independent experiments. *: $p < 0.05$; ***: $p < 0.001$; ns: not significant

AS-based method is qPCR. The determination of sample positivity in qPCR depends on the cycle at which amplified DNA is first detected, following method validation and interpretation guidelines. This is particularly crucial in addressing nonspecific amplifications that may occur at high cycle numbers [16]. We hypothesized that in this challenging low range of mutant allele frequencies, the sensitivity of CRISPR-Cas13a for the detection step may be different. Thus, AS regular PCRs were carried out, with the 3' nucleotide-specific primer hybridizing the mutant nucleotide and carrying an additional synthetic mismatch to inhibit the amplification of the *WT* allele (Supplemental Fig. 5a). AS-PCR was followed by CRISPR-Cas13a detection with crRNA-AS^{G12D} covering 15 nucleotides of the AS primer and 13 nucleotides of the amplified sequence (CASPER**,** Supplemental Fig. 5b). The fluorescence profile revealed full discrimination between the mutant and *WT* alleles (Fig. 5a). The maximal fluorescence ratio to the *WT* signal was 22.9 ± 8.8. This high discrimination translated into a high sensitivity of 0.5% (Fig. 5b), which was superior to that of conventional allele-specific PCR (Supplemental Fig. 5c) and equal to that of ddPCR (Supplemental Fig. 5d). Moreover, our strategy was quantitative for an MAF of up to 10%. A 4-parameter fit curve could be built, and a Spearman correlation analysis showed a significant *p*-value ($r^2 = 0.78$ and $r = 0.785$ with $p = 0.02$; Supplemental Fig. 5e, f).

CASPER for the detection of the KRAS^{G12D} mutation in pancreatic *cancer* patient liquid samples

To demonstrate the clinical feasibility of this assay, we analyzed fine needle aspiration fluid from 24 patients suspected of having PDAC (Fig. 5c)**.** All samples were first tested for *KRAS* G12/G13 mutations by ddPCR under routine laboratory conditions with a multiplex *KRAS*$^{G12/G13}$ mutation kit using conventional

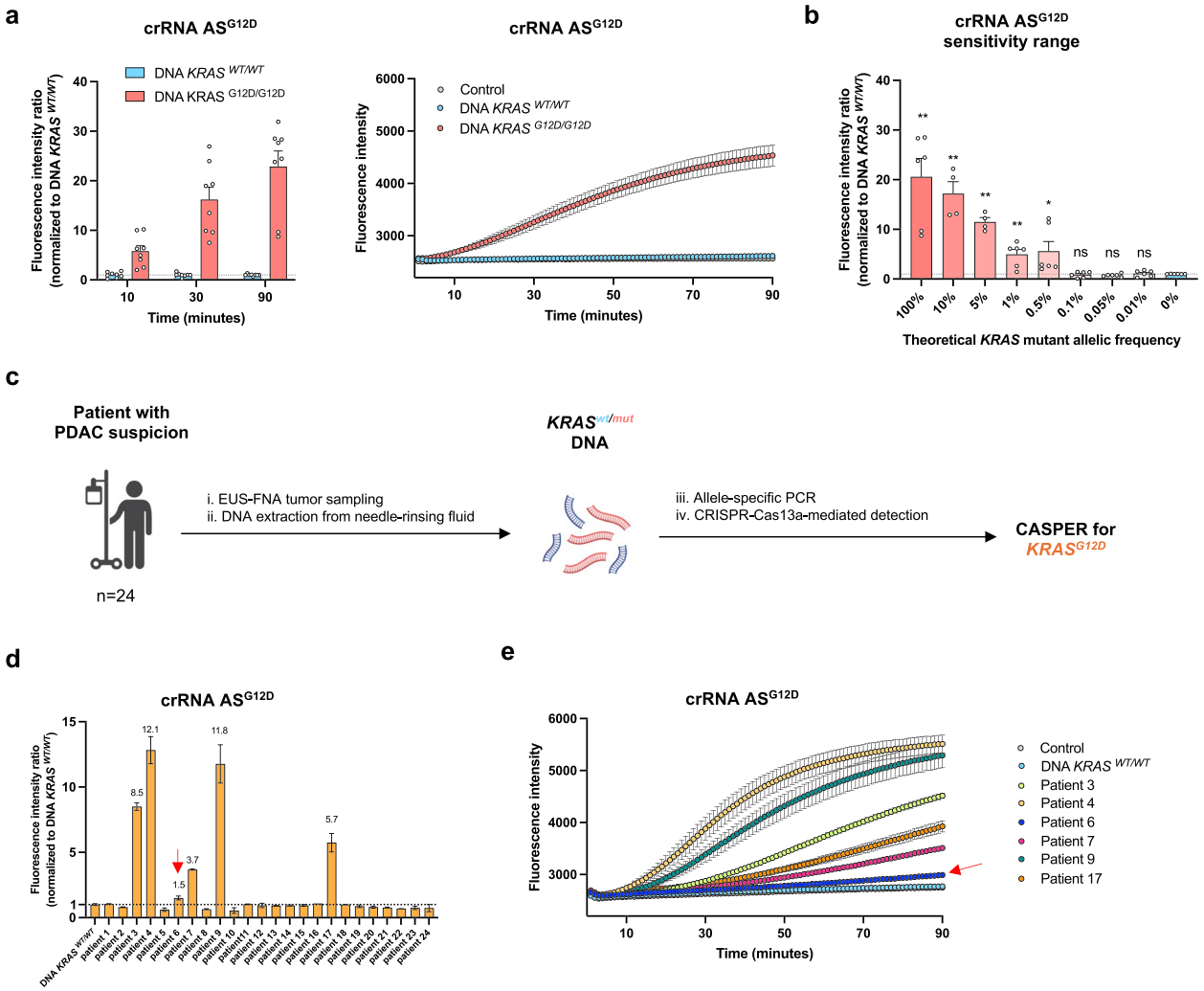

Fig. 5 CASPER for KRAS^{G12D} detection in patients' pancreatic fine needle aspiration samples. **a** Fluorescence ratio (left) and fluorescence level over time (right) in the presence of crRNA AS^{G12D} and PCR products from KRAS$^{G12D/G12D}$ or KRAS$^{WT/WT}$. **b** Quantification of the fluorescence ratio at 90 min in the presence of crRNA AS^{G12D} and PCR products from KRAS^{G12D} DNA diluted in KRAS^{WT} DNA. **a-b** Results are presented as the mean ± SEM with $n = 8$ (**a**) and $n = 6$ (**b**) replicates from independent experiments. **c** Experimental workflow for PDAC patient sample collection, sample processing, and KRAS^{G12D} detection with ddPCR and CASPER. **d** Quantification of the fluorescence ratio of PDAC patient samples at 90 min in the CASPER assay. The values at the top of the bars indicate the mean fluorescence intensity ratios, and the dotted lines indicate a fluorescence ratio of 1. **e** Quantification of the fluorescence level over time with the CASPER assay for the blank, WT control, and positive patient samples. **d-e** The red arrows point to the patient 6 results. The results are presented as the mean ± SD with $n = 2$ replicates from one experiment. *: $p < 0.05$; **: $p < 0.01$; ns: not significant

DNA input (Supplemental Fig. 6a and Supplemental Table 1). Eighteen samples (18/24, 75%) were found to be positive for one of the 7 *KRAS*$^{G12/G13}$ mutations included in the assay. Using the CASPER assay on the same 24 samples, we detected 6 *KRAS*^{G12D}–positive samples (Fig. 5d, e). The DNA inputs varied from 6 to 10 ng depending on the initial sample DNA concentration (Supplemental Table 1). All 6 samples were also positive according to the ddPCR multiplex *KRAS*$^{G12/G13}$ mutation test, with mutant allele frequencies ranging from 0.43% to 48.7% (Supplemental Fig. 6a). To confirm the detection of the CASPER-specific *KRAS*^{G12D} mutation, we tested 24 samples using a specific KRAS G12D ddPCR assay and identified 5 positive samples (Supplemental Fig. 6b). Noticeably, sample 6, which presented the lowest allelic frequency in the first ddPCR assay (0.43%, 39.7 ng DNA input), was positive with CASPER and negative with specific ddPCR using the same input of 10 ng DNA (red arrow). However, in the absence of available tumor tissue or sample leftover, we could not

confirm KRAS mutation identification by NGS. Finally, a 4-parameter fit curve analysis of the fluorescence intensity ratio and ddPCR-based $KRAS^{G12D}$ mutation allelic frequency showed that the CASPER assay was fully quantitative ($r^2 = 0.98$; Supplemental Fig. 6c).

Discussion

PDAC management is hindered by a lack of effective treatments and challenges in swiftly confirming the presence of tumors. This study is the first to test the ability of a conventional CRISPR-Cas13a platform to discriminate between $KRAS^{WT}$ and $KRAS^{MUT}$ alleles to detect low-frequency point mutations using limited DNA input. For this purpose, methods with high specificity and sensitivity are needed.

We first used crRNA guides with the 19th nucleotide of the spacer to hybridize the mutant position [13]. For in vitro *KRAS* allele discrimination, the position of the mismatch with the *WT* allele outside of the seed region was not ideal. Nonspecificity was also observed *in cellulo* [13], and the addition of another mismatch at position 14 marginally improved specificity. Guides mismatching the *WT* allele at positions 12 and 4 of the spacer did not allow full discrimination either. By testing different G12 mutation positions, our findings confirmed that a single mismatch in the guide spacer sequence distinctly influenced specificity [11, 17]. Indeed, heterocyclic purine/purine mismatches may create a local steric bulk that affects crRNA hybridization to the $KRAS^{WT}$ template more than purine/pyrimidine mismatches [18]. However, $crRNA^{G12D}$ (G/U mismatch on the *WT* allele) and $crRNA^{G12V}$ (G/A mismatch) showed similar profiles, while $crRNA^{G12C}$ (G/A) was more discriminant, confirming that the purine or pyrimidine status of the mismatch-related bases alone cannot explain the specificity variations. A recent study revealed another level of complexity showing that mismatch type, for example, A-G, displayed various specificities according to the position of the guanine nucleotide on the guide or the template [19]. The neighboring sequence likely contributes to specificity modulation [19]. Moreover, the concentrations of templates and RNA reporters could influence the fluorescence kinetics of Cas12 and Cas13 detection systems [20]. During the specificity assays, we used saturating amounts of DNA templates (*WT* or mutant) and RNA reporters. Thus, we believe that the $V_{max\ depends}$ only on the ability of the guide to efficiently hybridize with the template.

KRAS RNA templates adopt secondary structures leading to the formation of slightly different hairpin loops, rendering the sequence complementary to crRNAs more or less accessible (Supplemental Fig. 7a-d). The G12C mutation, which was best discriminated from the *WT* sequence, is in a stem, whereas the other mutations or the *WT* nucleotides are in loops. In addition, target RNA secondary structures may also need more energy for crRNA hybridization, augmenting the global Gibbs free energy of Cas13a activation [21]. This suggests that each template/guide couple may display distinct energetic properties, limiting the generalization of guidelines for crRNA design. Indeed, $crRNA\underline{19}^{G12D}$ and $crRNA\underline{4}^{G12D}$ were less discriminant than $crRNA\underline{12}^{G12D}$. By comparing the positioning of the 3 guides on the $KRAS^{G12D}$ RNA, we observed that secondary structures may affect crRNA hybridization (Supplemental Fig. 7e). The $crRNA\underline{4}^{G12D}$ and $crRNA\underline{19}^{G12D}$ hybridization zones fully covered stem-loop structures (lateral or terminal), which are only partly involved in the hybridization of $crRNA\underline{12}^{G12D}$. The additional energy required to separate the loop structure could therefore also affect crRNA hybridization, impacting target RNA detection [21]. Recent studies have reported that spacer sequence length also greatly influences crRNA hybridization and recognition properties [19]. While our work involved conventional 28-nucleotide spacer sequences, decreasing the spacer length could serve as a solution to limit nonspecific crRNA recognition. Notably, the link between crRNA-guided hybridization and Cas13a activation is also complex: strong hybridization of the crRNA with its target will not necessarily lead to strong nuclease activation, and vice versa [22]. Finally, 2 or 3 mismatches between the crRNA guide spacer and the target WT *KRAS* RNA sequence did not prevent nonspecific hybridization or Cas activation. As what is available for the design of primers and crRNA guides for the detection of viral sequences [23], or Cas13d guide design [24], large-scale and systematic studies are still required to setup guidelines optimizing Cas13a crRNA designed to detect and discriminate human sequences presenting single nucleotide variants.

Specificity was achieved by combining AS-PCR preamplification with CRISPR-Cas13a detection. Compared with conventional dye-based qPCR, fluorescence signal amplification, which is possible with Cas13a activation, made it possible to identify lower levels of PCR amplification. CASPER achieved similar or better sensitivity than ddPCR with low DNA input (6–10 ng), detecting one $KRAS^{G12D}$ ddPCR-false-negative patient. CASPER requires a conventional thermocycler with fluorescence detection, making it easy to implement as a complement to standard assays, especially when dealing with limited DNA input. $KRAS^{G12C}$ detection with high sensitivity but imperfect specificity was achieved by the Cas12 enzyme after PCR preamplification [25]. The initial amount of DNA input was not shared. Finally, building a $KRAS^{mut}$ CASPER panel, using multiple AS primers to multiplex mutation detection would enhance its diagnostic

accuracy and clinical applicability, providing a robust and complementary alternative to the established ddPCR gold standard. Additionaly, robust singleplex CASPER may improve clinical practice by identifying the druggable G12C [26] and G12D [27] *KRAS* mutations, even in cancers other than PDAC.

Conclusion

Given the low specificity and sensitivity of CRISPR-Cas13a for the detection of *KRAS* G12 point mutations, we implemented the CASPER assay, which enables specific and sensitive detection of $KRAS^{mut}$ alleles. We proved that this strategy is superior to qPCR and equal to ddPCR when using a small amount of input DNA and is thus compatible with challenging low-DNA quantity samples. The versatility of CASPER in terms of easy crRNA guide design and costless equipment could be a valuable solution for the production of personalized molecular tools that are adaptable to "hotspots" or less common mutations.

Supplementary Information

The online version contains supplementary material available at https://doi.org/10.1186/s13036-024-00450-3.

Supplementary Material 1.

Acknowledgements

We thank Omar Abudayyeh and Jonathan Gootenberg (Broad Institute of the Massachusetts Institute of Technology (MIT) and Harvard, Cambridge, MA 02142, USA) for sharing precious advice and help on CRISPR-Cas13a technology. The authors thank the staff of the CRISP'edit platform (TBMCore, University of Bordeaux, France) for assistance. We thank Sabine Berhouet, Severine Verdon, and Nicolas Faure for digital PCR technical assistance. We are also indebted to Stéphanie Lannelongue, Sandrine Hamon and Elsa Laraki for administrative assistance. We thank Anthony Cook for lab technical assistance.

Authors' contributions

S.A.: conceptualization (equal), funding acquisition (lead), investigation (lead), resources (lead), supervision (supporting), visualization (equal), writing – original draft (lead), writing – review and editing (equal) G.C.: conceptualization (equal), investigation (lead), visualization (equal), writing – original draft (equal), writing – review and editing (equal). L.K., J.R.: investigation (equal), writing – review and editing (equal) B.T.: conceptualization (equal), writing – review & editing (equal) V.P-M.: conceptualization (equal), writing – review & editing (equal). A.B., F.M-G.: writing – review & editing (equal) D.C.: conceptualization (supporting), writing – review & editing (equal) S.D.: conceptualization (equal), funding acquisition (lead), supervision (lead) writing – original draft (equal), writing – review & editing (lead).

Funding

This work was supported by the Association Française pour la Recherche sur le Cancer du Pancréas (AFRCP) and the Bordeaux University hospital.

Availability of data and materials

The raw data and their analysis are available upon request to the corresponding author.

Declarations

Ethics approval and consent to participate

This work was performed following the human and ethical principles of research outlined in the Helsinki guidelines and following local statutory requirements (acceptance of the study by the Bordeaux University Hospital ethics review board on 27/09/2023, reference CER-BDX 2023–102). Patients provided informed consent before EUS-FNA.

Consent for publication

Not applicable.

Competing interests

The authors declare no competing interests.

Received: 20 June 2024 Accepted: 19 September 2024
Published online: 01 October 2024

References

1. Gootenberg JS, Abudayyeh OO, Lee JW, et al. Nucleic acid detection with CRISPR-Cas13a/C2c2. Science. 2017;356:438–42.
2. Cullot G, Amintas S, Karembé L, et al. Specific High-Sensitivity Enzymatic Reporter UnLOCKing-Mediated Detection of Oncogenic BCR::ABL1 and EGFR Rearrangements. CRISPR J. 2023;6:140–51.
3. Storm AC, Lee LS. Endoscopic ultrasound-guided techniques for diagnosing pancreatic mass lesions: Can we do better? World J Gastroenterol. 2016;22:8658–69.
4. Gobbi PG, Bergonzi M, Comelli M, et al. The prognostic role of time to diagnosis and presenting symptoms in patients with pancreatic cancer. Cancer Epidemiol. 2013;37:186–90.
5. Herdeis L, Gerlach D, McConnell DB, et al. Stopping the beating heart of cancer: KRAS reviewed. Curr Opin Struct Biol. 2021;71:136–47.
6. Bailey P, Chang DK, Nones K, et al. Genomic analyses identify molecular subtypes of pancreatic cancer. Nature. 2016;531:47–52.
7. Bournet B, Selves J, Grand D, et al. Endoscopic ultrasound-guided fine-needle aspiration biopsy coupled with a KRAS mutation assay using allelic discrimination improves the diagnosis of pancreatic cancer. J Clin Gastroenterol. 2015;49:50–6.
8. Cazacu IM, Semaan A, Stephens B, et al. Diagnostic value of digital droplet polymerase chain reaction and digital multiplexed detection of single-nucleotide variants in pancreatic cytology specimens collected by EUS-guided FNA. Gastrointest Endosc. 2021;93:1142-1151.e2.
9. Mansour Y, Boubaddi M, Odion T, et al. Droplet digital polymerase chain reaction detection of KRAS mutations in pancreatic FNA samples: Technical and practical aspects for routine clinical implementation. Cancer Cytopathol. 2024;132(5):274–84.
10. Bryant KL, Mancias JD, Kimmelman AC, et al. KRAS: feeding pancreatic cancer proliferation. Trends Biochem Sci. 2014;39:91–100.
11. Kellner MJ, Koob JG, Gootenberg JS, et al. SHERLOCK: nucleic acid detection with CRISPR nucleases. Nat Protoc. 2019;14:2986–3012.
12. Buscail E, Alix-Panabières C, Quincy P, et al. High Clinical Value of Liquid Biopsy to Detect Circulating Tumor Cells and Tumor Exosomes in Pancreatic Ductal Adenocarcinoma Patients Eligible for Up-Front Surgery. Cancers. 2019;11:1656.
13. Zhao X, Liu L, Lang J, et al. A CRISPR-Cas13a system for efficient and specific therapeutic targeting of mutant KRAS for pancreatic cancer treatment. Cancer Lett. 2018;431:171–81.
14. Lázaro A, Maquieira Á, Tortajada-Genaro LA. Discrimination of Single-Nucleotide Variants Based on an Allele-Specific Hybridization Chain Reaction and Smartphone Detection. ACS Sens. 2022;7:758–65.
15. Milbury CA, Zhong Q, Lin J, et al. Determining lower limits of detection of digital PCR assays for cancer-related gene mutations. Biomol Detect Quantif. 2014;1:8–22.
16. Nolan T, Huggett J, Sanchez E. Good practice guide for the application of quantitative PCR (qPCR), LGC. 2013. Available online: https://www.gene-quantification.de/national-measurement-system-qpcr-guide.pdf.

17. Abudayyeh OO, Gootenberg JS, Konermann S, et al. C2c2 is a single-component programmable RNA-guided RNA-targeting CRISPR effector. Science. 2016;353:aaf5573.
18. Rossetti G, Dans PD, Gomez-Pinto I, et al. The structural impact of DNA mismatches. Nucleic Acids Res. 2015;43:4309–21.
19. Vargas AMM, Osborn R, Sinha S, et al. New design strategies for ultra-specific CRISPR-Cas13a-based RNA-diagnostic tools with single-nucleotide mismatch sensitivity. bioRxiv [Preprint]. 2023:2023.07.26.550755. https://doi.org/10.1101/2023.07.26.550755.
20. Huyke DA, Ramachandran A, Bashkirov VI, et al. Enzyme Kinetics and Detector Sensitivity Determine Limits of Detection of Amplification-Free CRISPR-Cas12 and CRISPR-Cas13 Diagnostics. Anal Chem. 2022;94(27):9826–34.
21. Ke Y, Huang S, Ghalandari B, et al. Hairpin-Spacer crRNA-Enhanced CRISPR/Cas13a System Promotes the Specificity of Single Nucleotide Polymorphism (SNP) Identification. Adv Sci. 2021;8:2003611.
22. Tambe A, East-Seletsky A, Knott GJ, et al. RNA-binding and HEPN-nuclease activation are decoupled in CRISPR-Cas13a. Cell Rep. 2018;24:1025–36.
23. Metsky HC, Welch NL, Pillai PP, et al. Designing sensitive viral diagnostics with machine learning. Nat Biotechnol. 2022;40:1123–31.
24. Wessels H-H, Méndez-Mancilla A, Guo X, et al. Massively parallel Cas13 screens reveal principles for guide RNA design. Nat Biotechnol. 2020;38:722–7.
25. Zhou H, Tsou J-H, Leng Q, et al. Sensitive Detection of KRAS Mutations by Clustered Regularly Interspaced Short Palindromic Repeats. Diagn Basel Switz. 2021;11:125.
26. Pfeiffer P, Qvortrup C. KRASG12C inhibition in colorectal cancer. Lancet Oncol. 2022;23:10–1.
27. Kemp SB, Cheng N, Markosyan N, et al. Efficacy of a Small-Molecule Inhibitor of KrasG12D in Immunocompetent Models of Pancreatic Cancer. Cancer Discov. 2023;13:298–311.

Publisher's Note